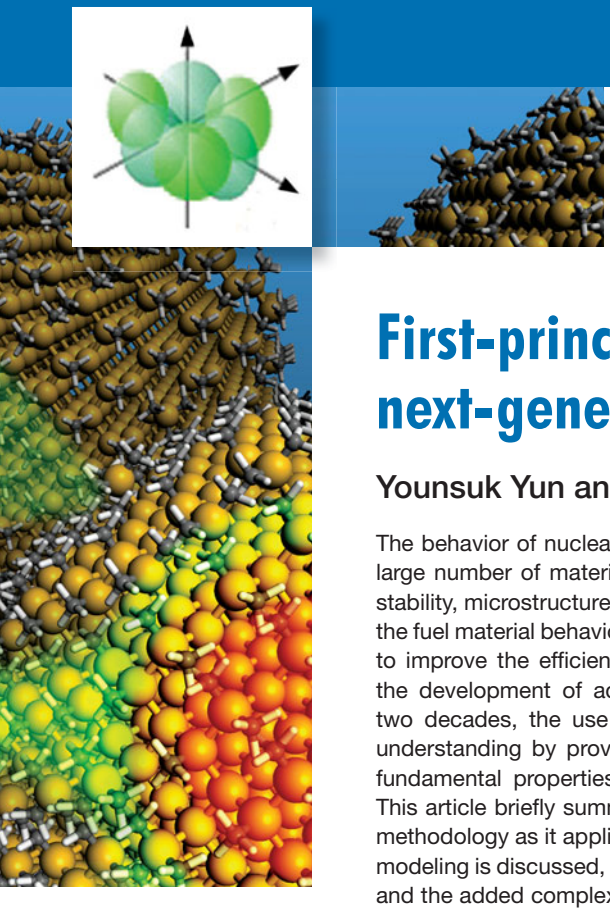


First-principles design of next-generation nuclear fuels

Younsuk Yun and Peter M. Oppeneer

The behavior of nuclear fuel in a reactor is a complex phenomenon that is influenced by a large number of materials properties, which include thermomechanical strength, chemical stability, microstructure, and defects. As a consequence, a comprehensive understanding of the fuel material behavior presents a significant modeling challenge, which must be mastered to improve the efficiency and reliability of current nuclear reactors. It is also essential to the development of advanced fuel materials for next-generation reactors. Over the last two decades, the use of density functional theory (DFT) has greatly contributed to our understanding by providing profound information on nuclear fuel materials, ranging from fundamental properties of *f*-electron systems to thermomechanical materials properties. This article briefly summarizes the main achievements of this first-principles computational methodology as it applies to nuclear fuel materials. Also, the current status of first-principles modeling is discussed, considering existing limitations and drawbacks such as size limitation and the added complexity associated with high temperature analysis. Finally, the future role of DFT modeling in the nuclear fuels industry is put into perspective.

Introduction

The ultimate performance of nuclear fuels is influenced by a host of materials properties, including thermomechanical strength, chemical stability, microstructure, and lattice defects. Overlaying this multitude of properties, nuclear fuels are exposed to a severe irradiation environment, which causes a continuous change of materials properties. Nuclear fuel behavior is therefore exceptionally rich, and a predictive understanding poses significant challenges. Experimental investigations of nuclear fuel materials, however, are very costly and, due to the risk of toxicity and radioactivity, are often restricted. Computational simulation and modeling can play a decisive role in the research on nuclear fuel materials, as first-principles modeling is now capable of providing precise, valuable insights and property data from an atomistic perspective. In fact, first-principles studies based on density functional theory (DFT) have already greatly contributed by supplying fundamental electronic-structure knowledge[1–8] and the material properties of defect-containing nuclear fuels.[9–20]

Among all fuel materials, UO_2 and PuO_2 have been most extensively studied both experimentally and computationally. This is especially true for UO_2, the standard nuclear fuel for light water reactors. PuO_2 has attracted interest because of its importance in mixed oxide fuel, $(U,Pu)O_2$, and as a radiotoxic ingredient of spent fuel. Various actinide compounds, including UC and U-Pu-C alloys, have also recently been investigated as candidate fuels for next-generation reactors.[20,21] The intricate nature of the 5*f* electrons in the actinides is crucial to understanding nuclear fuel properties such as chemical bonding, heat conductivity,[22] fission gas behavior,[11,12,14–19] and the surface interaction with molecules[23] relevant to fuel corrosion.[24] Hence, understanding actinide electronic structure is a prerequisite for understanding the behavior of nuclear fuel materials.

The local spin density approximation (LSDA) and the generalized gradient approximation (GGA) are most widely used in DFT-based first-principles calculations to estimate the exchange and correlation energy of electrons. The DFT provides an exact mapping of a many-electron system to a single-electron system, in which the electron moves in an effective potential; however, its exact form is not known. The unknown exchange-correlation potential is locally approximated in the LSDA by that of an electron in a homogeneous electron gas having the same density. The GGA is also a local approximation, but in addition, it takes the gradient of the electron density into account. Both approximations have been successfully applied to describe many of the fuel materials properties, despite their known limitation in capturing strong correlation effects of *f*-electrons.[25,26] In defect energy calculations, using DFT-LSDA/GGA Hamiltonians have

Younsuk Yun, Laboratory of Reactor Physics and Systems Behaviour, Paul Scherrer Institut, Switzerland; younsuk.yun@psi.ch
Peter M. Oppeneer, Department of Physics and Astronomy, Uppsala University, Sweden; peter.oppeneer@fysik.uu.se
DOI: 10.1557/mrs.2011.34

© 2011 Materials Research Society
https://doi.org/10.1557/mrs.2011.34 Published online by Cambridge University Press

provided results consistent with experimental data.[11–15] Taking spin polarization into account is of particular importance to 5*f* electrons in order to achieve accurate defect energies.[13,14] The success of predicting various nuclear fuel properties via a DFT-LSDA/GGA account of electron interactions can be explained by considering the energy scale of associated defect energies that are ~2–7 eV in UO_2.[11–15] This is much larger than the energy corrections that would properly account for strong electron correlation effects among the 5*f* electrons. A further complicating aspect of first-principles modeling applied to nuclear materials is that, on account of the large atomic mass of the actinide atoms, relativistic calculations need to be performed. In particular, the relativistic spin-orbit coupling can lead to shifts of ~1–2 eV in the energies of the 5*f* electrons.

In the following section, some of the main achievements of DFT modeling of nuclear fuels are reviewed. Subsequently, key requirements to improve DFT fuel calculations are discussed. The outlook of this methodology in future nuclear fuel materials design is examined in the last section.

Application of DFT to nuclear fuel characterization

Fundamental properties: UO_2

In addition to its technical importance as the standard nuclear fuel material, UO_2 has attracted interest as a prototypical actinide compound to investigate the intriguing behavior of *f*-electrons in an open 5*f* shell. UO_2 crystallizes in the cubic fluorite CaF_2 structure and develops antiferromagnetic order below 30 K.[3,19,25] Various DFT studies have been conducted to investigate basic properties of UO_2, including its structural, chemical, thermodynamic, electronic, and magnetic properties.[1–8] In particular, advanced DFT-based approximations beyond the LSDA and GGA, such as LSDA/GGA+*U*,[25,26] hybrid functionals,[5,27,28] self-interaction correction (SIC),[29,30] and DFT+DMFT (dynamical mean field theory) approaches,[22] have been developed to correctly capture the strong correlations of 5*f* electrons in UO_2 that are responsible for its insulating behavior with a bandgap energy of about 2 eV. **Figure 1** shows calculated *m*-decomposed partial *f*-electron density of states (PDOS) of UO_2 obtained from GGA+*U* calculations.[6] The PDOS explains the role of the 5*f* electrons in the U–O bonding in conjunction with antiferromagnetic ordering in UO_2.

The diagram at the bottom shows the seven 5*f*, $m = -3$ to 3 orbitals.[31] Among these orbitals, four spin-up orbitals ($m = -3,-1,1,3$) are partially occupied in UO_2 with lobes directed along either the *x*- or *y*-axis in the coordinate system and without a nodal plane perpendicular to the *z*-axis. The four 5*f* PDOS peaks are coincident with peaks in the O *p*-DOS (i.e., these four 5*f* orbitals hybridize with O $2p_x$ and $2p_y$ orbitals).[6] The electronic structure of UO_2 is still a challenging topic, and comprehensive DFT studies are being conducted that consider spin-orbit and crystal field effects in order to investigate the crystal field levels and non-collinear magnetic structure of UO_2.[32]

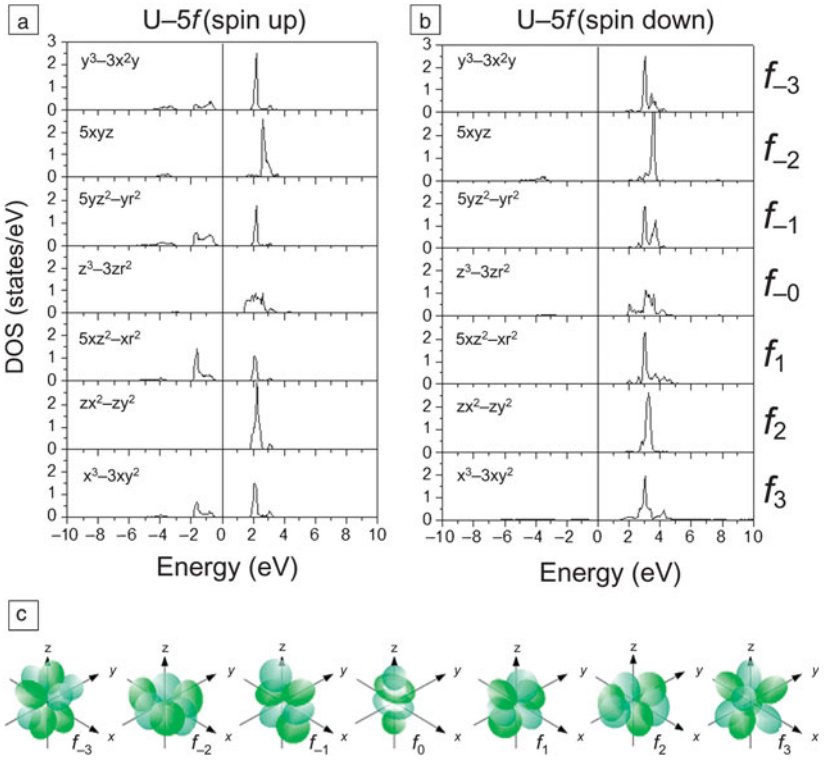


Figure 1. (a) Spin up and (b) spin down *m*-orbital decomposed partial electron density of states (PDOS) of the uranium 5*f* electrons in UO_2. (c) Sketch of the seven 5*f* orbitals.[31] The first-principles calculations provide detailed information on the chemical bonding between uranium and oxygen.

Materials properties

Defects

Defects are central to an understanding of atomic transport in nuclear fuels. In particular, it is known that point defects form a major diffusion channel for fission gas atoms in the fuel matrix. To model defect-containing materials, a supercell approach is required. A 2 × 2 × 2 supercell containing 96 atoms has been predominantly used in recent DFT calculations.[12–19] **Figure 2a** shows the oxygen sublattice in a 2 × 2 × 2 supercell of cubic UO_2, ThO_2, and PuO_2. The oxygen atoms are located at the corners of each cube, and actinide atoms are located at the center of alternative grey cubes.

Table I reports formation energies of major intrinsic defects in UO_2. Here an oxygen Frenkel pair consists of an oxygen interstitial and vacancy, and a Schottky trio defect consists of one uranium vacancy and two oxygen vacancies formed in the UO_2 lattice. The five computed energies were obtained using DFT-based methods and a 2 × 2 × 2 supercell. Most of the calculated values are in

https://doi.org/10.1557/mrs.2011.34 Published online by Cambridge University Press

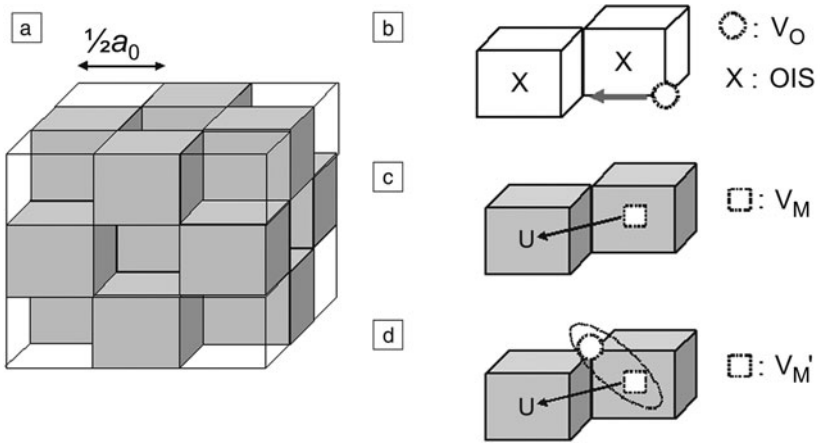


Figure 2. (a) Oxygen sublattice of a 2 × 2 × 2 supercell of actinide dioxides; (b) the migration of an oxygen vacancy V_O between two adjacent lattice sites; (c) the migration of an actinide vacancy V_M (M = U or Th); (d) the migration of an actinide vacancy V_M' due to the effective movement of a joint vacancy, V_{MO}. OIS, octahedral interstitial site; a_0, lattice parameter.

good agreement with the experimental data (last column), which illustrates that parameter-free DFT calculations are reliable and accurate within an acceptable error range. Another important achievement of DFT studies is the improved understanding of atomistic diffusion. **Table II** gives DFT-computed migration energies of single vacancies in UO_2 and ThO_2. The migration energy was calculated from the energy difference between an initial configuration and a saddle point when a M (U or Th) or O vacancy, denoted V_M or V_O, respectively, moves from its initial lattice site to the nearest adjacent site, as shown in Figure 2b. The migration energy of V_U is calculated to be almost 50% higher than the experimental value, whereas that of V_O agrees very well. However, the overestimated result for V_U can be explained by considering the effective movement of a combined U and O vacancy, V_{UO}, as depicted in Figure 2d. The migration energy of V_U is reduced by about 1 eV due to the existence of an adjacent V_O. Hence, the calculations predict a detailed atomistic process in which an oxygen vacancy plays an important role to enhance the mobility of a uranium vacancy in UO_2. The migration energies of single vacancies in ThO_2 (see Table II) are predicted to be significantly higher than those in UO_2.[15] The assisting influence of a V_O was not observed in the movement of a Th vacancy. DFT studies thus predict that point defects are less easily created as well as less mobile in ThO_2 than in UO_2.

The diffusion of fission gases in the fuel matrix is closely connected to lattice defects, as these defects are known to act as a major diffusion channel of fission gas atoms. Therefore, based on the defect energetics, it is expected that fission gas atoms are less mobile in ThO_2 than in UO_2. Further calculations were conducted to understand diffusion behavior of fission gas atoms in ThO_2 and UO_2, and it was reported[15] that Xe, which is one of the highest fractional released fission gases in UO_2, is more likely to diffuse in UO_2 than in ThO_2. **Figure 3a and 3b** show the electron charge distribution of UO_2 and ThO_2, respectively, and clearly illustrate the different behavior of Xe in the two oxides. In Figure 3a, Xe with index (1) is initially at V_U, and subsequently is seen to move during atomic relaxation when a V_O (2) is created at the nearest lattice site. In contrast, in ThO_2, Xe remains at the initial position of V_{Th} during atomic relaxation, despite the creation of a new V_O nearby, as shown in Figure 3b. A detailed schematic diagram depicting the Xe behavior in the two dioxides is plotted on the right side in Figure 3.

In UO_2, the barrier-less movement of Xe during atomic relaxation is due to the strain energy of Xe caused by its relatively large atomic radius (Xe = 2.15 Å, U^{4+} = 1.01 Å, Th^{4+} = 1.07 Å).[33] However, the strain-energy effect of Xe seems not enough to cause Xe movement in ThO_2. This is mainly associated with the strong resistance of Th against variation of its valency in ThO_2. Th in ThO_2 is most stable with 4+ valency, and electron redistribution is energetically unfavorable, which affects the formation and mobility of defect atoms and the diffusion of Xe atoms. These DFT results are supported by experiments showing that the Xe release is lower in UO_2 mixed with ThO_2, $(U,Th)O_2$[34] than in UO_2. It is very important to understand the diffusion mechanism of fission gases in nuclear fuels, because fission gas is one of the parameters that severely affects fuel safety conditions, such as fuel swelling, thermal conductivity, and fuel rod pressure after it is released into the gap between fuel pellet and cladding. Controlling fission gas release is therefore a crucial factor to increase nuclear fuel burnup, which is the degree to which the fuel material is consumed in the nuclear reactor so that the fuel efficiency is improved. First-principles studies investigating the trap sites and diffusion mechanism of fission gases reported that Xe atoms prefer to accommodate the charge neutral UO_2 trivacancy among existing interstitial sites and various vacancies due to its charge neutrality as well as its large size, which are suitable to accommodate the large atomic radius of Xe.[33,35] The trivacancy was moreover computed to play a central role in the Xe diffusion in UO_2 through the successive process of dissociation and association of the Xe-trivacancy complex,[12] as shown in **Figure 4**.

It should be mentioned that accurate atomic transport modeling is a challenge

Table I. Calculated and experimental formation energies in eV of intrinsic defects in UO_2.

	Yun et al.[15]	Iwasawa et al.[16]	Gupta et al.[17]	Nerikar et al.[18]	Dorado, Freyss[19]	Experimental[35]
O Frenkel pair	4.5	4.1	4	3.9	3.1	3.0–4.6
Schottky trio	7.2	–	7.2	7.6	4.5	6.0–7.0

The calculated results[16–19] were obtained using the generalized gradient approximation with added Coulombic correlation (GGA+*U*) approach, except for the results[15] obtained using GGA.

https://doi.org/10.1557/mrs.2011.34 Published online by Cambridge University Press

Table II. Computed[12,15] and experimental[33] migration energies E_m in eV.

	$E_m(V_O)$	$E_m(V_M)$	$E_m(V_M)'$
UO_2 (calc)	0.63	3.09	2.19
UO_2 (exp)	0.50	–	2.40
ThO_2 (calc)	1.27	4.47	4.47

V_O and V_M indicate oxygen and actinide atom vacancies (M = Th or U), respectively, and $E_m(V_M)'$ indicates the effective migration energy of an M-vacancy within the joint V_M and V_O movement.

in DFT research, as it is necessary to take temperature effects into account to achieve close energy values. Supercell size is also a sensitive parameter that affects energy calculations required for atomic transport; this aspect will be discussed in more detail later.

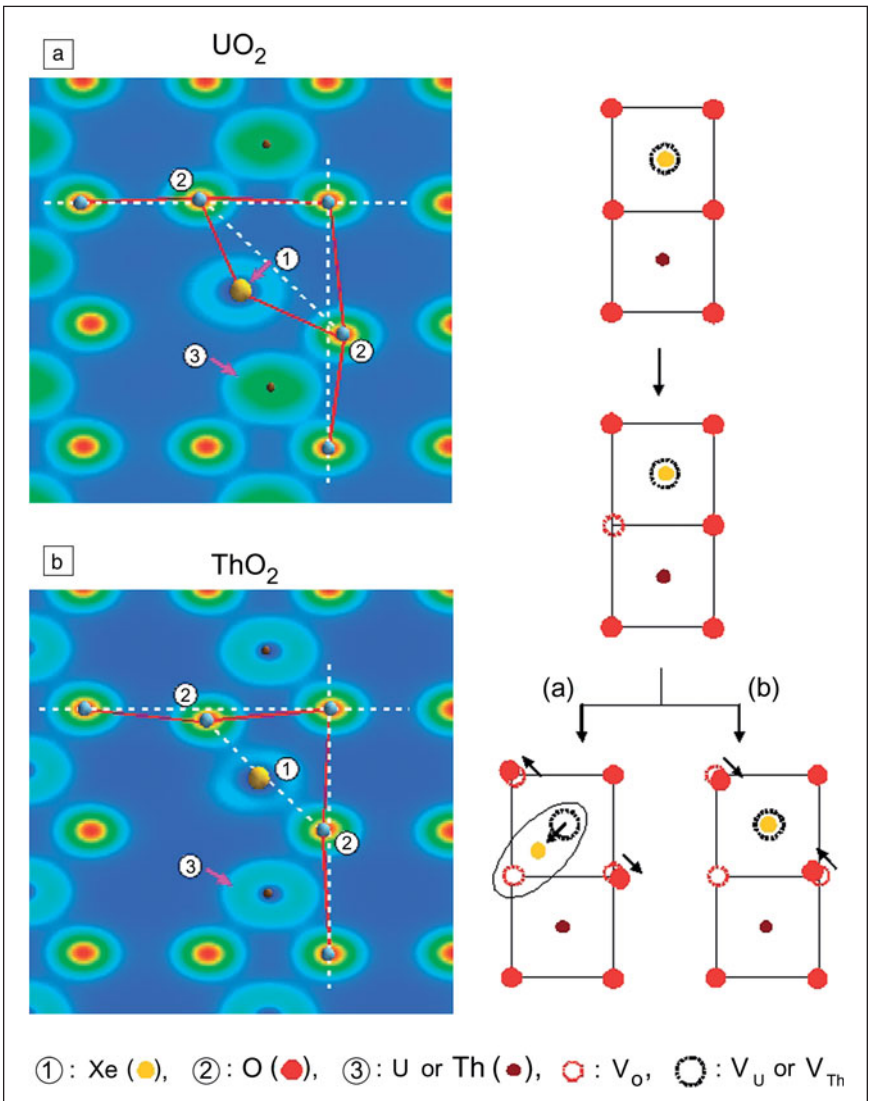


Figure 3. Electron charge distribution of Xe-V_{MO} complex obtained through atomic relaxation in (a) UO_2 and (b) ThO_2. The magnitude of the electron density is indicated by a color grading, where red is used for the highest electron density and blue for the lowest one. Xe moves from the initial position at V_U to the center of V_{UO} when a V_O is created at the nearest lattice site, while in (b), it remains at the initial position of V_{Th}, despite the creation of a new V_O nearby. These processes are schematically explained in the right-hand panel.

Thermodynamic behavior

The heat transfer from the fuel to the coolant is the central process to generate electricity from nuclear power. Knowledge of the fuel's thermodynamic properties is therefore essential to model the fuel's behavior under operation conditions at high temperatures. First-principles methods are increasingly being used to determine the thermodynamic properties of nuclear fuels. Recently, a DFT+DMFT study of the lattice dynamical properties of UO_2 and PuO_2 (i.e., their phonon spectra) was reported.[22] The calculations suggested that an improved thermal conductivity of the fuel could be achieved through dedicated materials design, building on the observation that dispersive longitudinal optic phonon modes do not contribute to the heat transfer.[22] Thus far, however, only a few DFT-based calculations of the phonon spectrum of actinide materials have been performed, employing either the linear response theory[22,36] or the direct approach.[37,38] In the former approach, a perturbation of the atomic positions with the periodicity of the original lattice is treated with standard perturbation theory, and first-order corrections are computed. In the direct approach, or so-called supercell method, a finite displacement of several atoms in a supercell is employed to compute atomic force constants and the phonon spectrum. In this direct approach, it is important to achieve convergence of phonon frequencies with respect to supercell size. Generation of such data would be a valuable step for characterizing the thermal properties of nuclear fuels. An alternative first-principles approach is to use DFT to compute interatomic potentials, which are subsequently used in molecular dynamics (MD) simulations. This approach has already been successfully applied to describe the thermal expansion of dioxide fuels[39] and the next-generation fuel uranium nitride (UN).[40]

DFT calculations on nuclear fuel: Computational costs

The computationally heaviest step in DFT calculations for nuclear fuel materials is to perform the self-consistent field (SCF) total energy minimization (i.e., the iterative calculation of single-particle wave functions and the effective potential that depends on these wave functions until the starting and evaluated potential match). The costs of the SCF calculation depend mainly on the number of atoms in the chosen simulation cell. To obtain the electronic structure, cohesive properties, and magnetic properties,

https://doi.org/10.1557/mrs.2011.34 Published online by Cambridge University Press

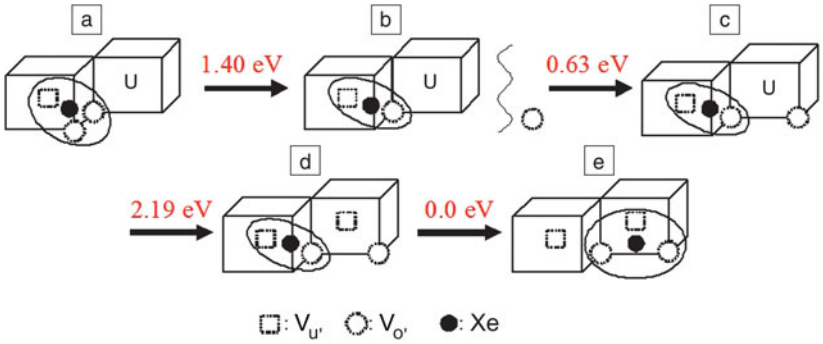


Figure 4. (a) Structure of a Xe-trivacancy complex, (b) dissociation of V_O from a Xe-trivacancy with binding energy of about 1.4 eV, (c) combination of a new V_O with the migration energy of 0.63 eV, (d) migration of V_U with the help of the nearest V_O with a migration energy of 2.19 eV, (e) formation of a new Xe-trivacancy complex by the spontaneous movement of Xe due to strain energy in the UO_2 lattice.[9]

a calculation for a single unit cell suffices, and the required computation time is usually less than a few hours for the convergence of the SCF total energy with a single CPU. **Table III** shows the imposed parameter values and the computation time to calculate the electronic structure of UO_2. A tetragonal unit cell is used to model antiferromagnetically ordered UO_2, which consists of two U atoms with antiparallel magnetic moments and four O atoms. Once the self-consistent electronic charge density and wave functions are computed, other elements of the electronic structure, such as the electronic density of states and energy band structure, can be computed quickly.

The use of a large simulation cell is essential for defect-related calculations, such as formation and migration energy of defects. The computation time required increases approximately as $\sim N^3$, with N being the number of atoms in the simulation cell. Moreover, to simulate a system with defects, all atomic positions in the system have to be relaxed to obtain the overall minimal energy configuration. This implies that all atomic positions must be optimized until the forces acting on each of the atoms in the supercell vanish. This is usually an extremely time-consuming task. Table III summarizes the computational details for the calculation of the formation energy of a uranium vacancy V_U in UO_2 using the $2 \times 2 \times 2$ supercell. The number of used CPUs was determined by carrying out an optimization test for the parallel computing platform. From Table III, it can be seen that the complete SCF total energy convergence with structural optimization requires a considerable computation time of 57 hours. Hence, the computational costs to simulate defect diffusion in nuclear fuels are massive. The reduction of computational costs is therefore an important key to increase the impact of first-principles techniques for nuclear fuel modeling. Nonetheless, in spite of the considerable computational efforts required, the costs of performing experimental studies on nuclear fuel materials are unequivocally higher.

Limitations and improvements to DFT modeling

Several challenges are currently encountered in analyses of nuclear fuels using DFT. The first area that requires additional research is extensions and improvements of the DFT+*U* methodology, since 5*f* states in actinide oxides are strongly correlated. Here, the *U* indicates the effective interaction parameter that is added to correct the on-site Coulomb repulsion interaction of the 5*f* electrons. The DFT+*U* method has become an important approximation in the study of nuclear fuel materials. It is, from a numerical perspective, a relatively simple extension beyond the standard GGA and can be applied in parallel computations to treat supercells with a large number of atoms. However, the DFT+*U* functional has the weakness that, depending on the initial density matrix in the self-consistent cycle, one can converge to a metastable state instead of the ground state.[7] A solution to this problem could be the recently proposed

Table III. Computational details for self-consistent field (SCF) calculations of antiferromagnetic UO_2 using the VASP (Vienna *ab initio* simulation package) code.[45]

	PAW-GGA+*U* (SOC included)	PAW-GGA calculation
Number of atoms in simulation cell	6 atoms: 2 U and 4 O	96 atoms: 32 U and 64 O
Planewave cutoff energy	500 eV	500 eV
Number of k-points in the Brillouin zone	6 × 6 × 4 (72 irreducible k-points)	2 × 2 × 2 (4 irreducible k-points)
Criterion for SCF energy convergence	10^{-5} eV	10^{-5} eV
Criterion for atomic force relaxation convergence	—	0.01 eV/Å
Computer platform	1 CPU (4 GB RAM)	32 CPUs (4 GB RAM each)
Computation time	4568.75 seconds (~1.26 hours)	211869.48 seconds (~56.85 hours)

The VASP code is an *ab initio* quantum mechanical calculation code using pseudopotentials and a plane-wave basis set. First column: The total energy calculation performed with the projector augmented wave (PAW) method and with spin-orbit coupling (SOC) and an additional Coulomb correlation *U* included. Second column: The formation energy of a uranium vacancy V_U using the PAW-GGA (generalized gradient approximation) method. The calculation includes relaxation of all atomic positions in the supercell until all atomic forces are minimized.

https://doi.org/10.1557/mrs.2011.34 Published online by Cambridge University Press

density-matrix controlling scheme,[8] which was successfully applied to reach the ground state of UO_2. The density-matrix controlling scheme is a definite improvement to correctly determine the ground state of actinide oxides within DFT+*U* calculations and could have a significant and positive impact on fuel materials research. However, it has not been applied yet for lattice defect calculations in a supercell. In addition to improvements of the DFT+*U* functional, it is also necessary that other approximations to the Hamiltonian, such as hybrid functionals,[27,28] SIC,[29,30] and DFT+DMFT, [22] be tested and developed further to calculate nuclear fuel materials, in combination with the development of parallelized versions of these approaches appropriate to the analyses associated with supercell domains.

A second demand on DFT-based techniques is to provide a better characterization of temperature-dependent properties in nuclear fuels. For many fuel materials properties, it is essential to take temperature-dependent effects into account. For example, fission gas diffusion occurs dominantly at temperatures over 1000°C.[33] Nonetheless, standard DFT calculations can provide acceptable results for fission gas behavior.[11,12,14,15,19] For instance, the migration energy of Xe between two interstitial sites was calculated as 4.69 eV,[14] and this agrees with experimental data of 3.90 eV within 20%.[33] However, when expansion of the lattice was accounted for, it was found that the migration energy was reduced to 3.78 eV,[14] which calls into question the validity of the nominal result. Mermin[41] generalized the Hohenberg-Kohn theorem (that a many-electron problem can be exactly mapped to a single-electron problem) to finite temperatures. Temperature-dependent DFT has been successfully applied to describe materials behavior over a wide range in temperature, up to almost 1000ºC.[11,12,14,15,19] Using temperature-dependent DFT in combination with MD simulations, Mattsson et al.[42] computed the anomalous temperature evolution of the vacancy formation energy in Mo up to about 2700ºC, and Root et al.[43] studied xenon's behavior at extreme conditions of high pressure and high temperature. Although *T*-dependent (temperature dependent) DFT can thus be employed to high-temperature dynamic and thermodynamic properties, it has not yet been applied to nuclear materials. Standard DFT-based MD simulations have already been performed.[42–44] These are, for example, well-suited to investigate the important role of fission gas diffusion[11,12,14,15,19] in the nuclear fuel. DFT-based MD simulations[44] of the temperature-dependent diffusion coefficient and pathway were reported for UO_2. Furthermore, the defect jump rate and absolute concentration can be calculated as a function of temperature using the DFT-based MD.[42] MD is implemented in several DFT simulation packages.[45,46]

Current limitations on supercell size are a third area deserving of research attention. The scale of DFT-based modeling is, in general, limited to cells of the order of a few hundred atoms, and this limits the types of defect structures and interactions that may be considered. For example, to calculate the migration energy of fission gas atoms in a dilute concentration, a reasonably large supercell, consisting approximately of *N* times the unit cell for a defect concentration of 1/*N*, is needed to model a system containing several defects well separated from each other; otherwise, the defect-defect interaction between adjacent cells will be too large to obtain accurate energy values. Suitable supercell sizes can be determined from the geometry optimization of the supercell containing defects by carrying out total energy convergence tests, including atomic relaxation as a function of supercell size (i.e., the lattice coordinates of all the atoms in the supercell are modified during the total energy calculation until they converge to their equilibrium positions that are defined by the criterion that the forces acting on each atom are smaller than a lower value, usually 0.01 eV/Å). An efficient approximation has been developed recently that allows larger system sizes to be considered, allowing for an analysis of dislocation and dislocation-solute physics.[47] A 540-atom supercell was used with periodic boundary conditions to the dislocation line direction. To improve computational efficiency for such a huge number of atoms, the cell was divided into three regions, and forces in the separate regions were relaxed, subject to a consideration of the long-range elastic response of the material.

Along with the development of algorithms focused on defects and actinides, it is also important to improve computational performance capacity through the development of efficient parallel computing algorithms. While not strictly focused on nuclear fuels, such generic improvements to DFT methodology may prove to have the largest impact of all on the ability to consider large numbers of atoms.

Summary and future role of DFT techniques in nuclear fuel research

First-principles modeling is now widely accepted as a tool not only to develop advanced fuels with improved efficiency in current reactors but also to design nuclear fuel materials of the future.[48] As already noted, for instance, density functional theory (DFT) studies predict that ThO_2 possesses qualities superior to UO_2 with regard to chemical stability and defect dynamics. Nitrides such as (U,Pu,MA)N and (Pu,MA,Zr)N, where MA is a minor actinide, are now being investigated using DFT as promising advanced nuclear fuel because of their high thermal conductivity and high melting point.[49] In a recent DFT study, point defects in uranium mononitride were investigated, calculating the defect formation energy as well as defect-induced electronic density redistribution.[50,51] Uranium monocarbide and ternary alloys, including U-Pu-C, are now considered as possible candidates for next-generation reactor fuels because of the combination of a high melting temperature and high actinide density,[20,21] and first-principles calculations have been performed to investigate the thermodynamic properties and phase diagram of these alloys.[21] Advanced DFT modeling can already provide valuable knowledge regarding the existence of potential candidate materials before experimental data, such as structure and basic properties.

During the last few decades, first-principles calculations performed within the framework of DFT have had a tremendous and positive impact on nuclear fuels research. It has become

https://doi.org/10.1557/mrs.2011.34 Published online by Cambridge University Press

evident that DFT can significantly contribute to the nuclear energy industry by providing both insights and quantitative property data associated with fuel performance. Parameter-free DFT calculations have not only improved the reliability and accuracy of computed materials properties, but they also contributed to a better understanding of the microstructural character of nuclear fuels. However, the current DFT techniques need further improvement, with the primary need being associated with the ability to scale up to larger numbers of atoms and to develop finite temperature predictions of material behavior.

Acknowledgments

The Swedish Nuclear Fuel and Waste Management Company, SKB, and the European Commission have supported this work. The authors acknowledge valuable discussions with Kwangheon Park, Hanchul Kim, Olle Eriksson, and Lars Werme.

References

1. S.L. Dudarev, G.A. Botton, S.Y. Savrasov, C.J. Humphreys, A.P. Sutton, *Phys. Rev. B* **57**, 1505 (1998).
2. K.N. Kudin, G.E. Scuseria, R.L. Martin, *Phys. Rev. Lett.* **89**, 266402 (2002).
3. R. Laskowski, G.K.H. Madsen, P. Blaha, K. Schwarz, *Phys. Rev. B* **69**, 140408(R) (2004).
4. Y. Yun, H. Kim, H. Kim, K. Park, *Nucl. Eng. Technol.* **37**, 293 (2005).
5. I.D. Prodan, G.E. Scuseria, R.L. Martin, *Phys. Rev. B* **76**, 033101 (2007).
6. Y. Yun, H. Kim, H. Lim, K. Park, *J. Korean Phys. Soc.* **50**, 1285 (2007).
7. B. Amadon, F. Jollet, M. Torrent, *Phys. Rev. B* **77**, 155104 (2008).
8. B. Dorado, B. Amadon, M. Freyss, M. Bertolus, *Phys. Rev. B.* **79**, 235125 (2009).
9. D.A. Anderson, J. Lezama, B.P. Uberuaga, C. Deo, S.D. Conradson, *Phys. Rev. B* **79**, 024110 (2009).
10. M. Freyss, T. Petit, J.P. Crocombette, *J. Nucl. Mater.* **347**, 44 (2005).
11. M. Freyss, N. Vergnet, T. Petit, *J. Nucl. Mater.* **352**, 144 (2006).
12. Y. Yun, H. Kim, H. Kim, K. Park, *J. Nucl. Mater.* **378**, 40 (2008).
13. Y. Yun, O. Eriksson, P.M. Oppeneer, *J. Nucl. Mater.* **385**, 510 (2009).
14. Y. Yun, O. Eriksson, P.M. Oppeneer, *J. Nucl. Mater.* **385**, 364 (2009).
15. Y. Yun, P.M. Oppeneer, H. Kim, K. Park, *Act. Mater.* **57**, 1655 (2009).
16. M. Iwasawa, Y. Chen, Y. Kaneta, T. Ohnuma, H.-Y. Geng, M. Kinoshita, *Mater. Trans.* **47**, 2651 (2006).
17. F. Gupta, G. Brillant, A. Pasturel, *Philos. Mag.* **87**, 2561 (2007).
18. P. Nerikar, T. Watanabe, J.S. Tulenko, S.R. Phillpot, S.B. Sinnott, *J. Nucl. Mater.* **384**, 61 (2009).
19. B. Dorado, M. Freyss, G. Martin, *Eur. Phys. J. B* **69**, 203 (2009).
20. N. Vigier, C. Den Auwer, C. Fillaux, A. Maslennikov, H. Noël, J. Roques, D.K. Shuh, E. Simoni, T. Tyliszczak, P. Moisy, *Chem. Mater.* **20**, 3199 (2008).
21. M. Freyss, *Phys. Rev. B* **81**, 014101 (2010).
22. Q. Yin, S.Y. Savrasov, *Phys. Rev. Lett.* **100**, 225504 (2008).
23. M.N. Huda, A.K. Ray, *Phys. Rev. B* **72**, 085101 (2005).
24. F.N. Skomurski, R.C. Ewing, A.L. Rohl, J.D. Gale, U. Becker, *Am. Mineral.* **91**, 1761 (2006).
25. S.L. Dudarev, D. Nguyen Manh, A.P. Sutton, *Philos. Mag. B* **75**, 613 (1997).
26. Y. Baer, J. Schoenes, *Solid State Commun.* **33**, 885 (1980).
27. K.N. Kudin, G.E. Scuseria, R.L. Martin, *Phys. Rev. Lett.* **89**, 266402 (2002).
28. R. Atta-Fynn, A.K. Ray, *Europhys. Lett.* **85**, 27008 (2009).
29. L. Petit, A. Svane, Z. Szotek, W.M. Temmerman, *Science* **301**, 498 (2003).
30. L. Petit, A. Svane, Z. Szotek, W.M. Temmerman, G.M. Stocks, *Phys. Rev. B* **81**, 045108 (2010).
31. R.H. Petrucci, W.S. Harwood, G. Herring, *General Chemistry: Principles and Modern Applications* (Prentice Hall, New Jersey, 2001).
32. F. Zhou, V. Ozoliņš, "Crystal field and magnetic structure of UO_2"; http://lanl.arxiv.org/abs/1006.3988
33. Hj. Matzke, *Diffusion Processes in Nuclear Materials* (North Holland, Amsterdam, 1992).
34. H. Kim, K. Park, Y. Yun, B.G. Kim, H.J. Ryu, K.C. Song, Y.S. Choo, K.P. Hong, *Ann. Nucl. Energy* **34**, 153 (2007).
35. Hj. Matzke, *J. Chem. Soc. Faraday. Trans.* 2 **83**, 1121 (1987).
36. X. Dai, S.Y. Savrasov, G. Kotliar, A. Migliori, H. Ledbetter, E. Abrahams, *Science* **300**, 953 (2003).
37. K. Parlinski, PHONON software, Cracow, Poland, 2005.
38. P. Piekarz, K. Parlinski, P.T. Jochym, A.M. Oles, J.-P. Sanchez, J. Rebizant, *Phys. Rev. B* **72**, 014521 (2005).
39. K. Yamada, K. Kurosaki, M. Uno, S. Yamanaka, *J. Alloys Compd.* **307**, 10 (2000).
40. P.H. Chen, X.L. Wang, X.C. Lai, G. Li, B.Y. Ao, Y. Long, *J. Nucl. Mater.* **404**, 6 (2010).
41. N.D. Mermin, *Phy. Rev.* **137**, A1441 (1965).
42. T.R. Mattsson, N. Sandberg, R. Armiento, A.E. Mattsson, *Phys. Rev. B* **80**, 224104 (2009).
43. S. Root, R.J. Magyar, J.H. Carpenter, D.L. Hanson, T.R. Mattsson, *Phys. Rev. Lett.* **105**, 085501 (2010).
44. K. Govers, S. Lemehov, M. Hou, M. Verwerft, *J. Nucl. Mater.* **395**, 131 (2009).
45. VASP, http://cms.mpi.univie.ac.at/vasp.
46. CP2K, http://cp2k.berlios.de.
47. D.R. Trinkle, C. Woodward, *Science* **310**, 1665 (2005).
48. R.W. Grimes, R.J.M. Konings, L. Edwards, *Nat. Mater.* **7**, 683 (2008).
49. H. Muta, K. Kurosaki, M. Uno, S. Yamanaka, *J. Mater. Sci.* **43**, 6429 (2008).
50. E.A. Kotomin, R.W. Grimes, Y. Mastrikov, N.J. Ashley, *J. Phys. Condens. Matter* **19**, 106208 (2007).
51. Y. Lu, B.-T. Wang, R.-W. Li, H. Shi, P. Zhang, *J. Nucl. Mater.* (2011), in press. □





https://doi.org/10.1557/mrs.2011.34 Published online by Cambridge University Press